

Very large-scale structures observed in DNS of turbulent channel flow with passive scalar transport

H. Kawamura¹, H. Abe² and Y. Matsuo²

¹Department of Mechanical Engineering
Tokyo University of Science, Noda-shi, Chiba, 278-8510 JAPAN

²Information Technology Center
Japan Aerospace Exploration Agency, Jindaiji-higashi, Chofu, Tokyo 182-8522 JAPAN

Abstract

Direct numerical simulation of a fully developed turbulent channel flow with passive scalar transport has been carried out at four Reynolds numbers, 180, 395, 640 and 1020, based on the friction velocity and the channel half width. The molecular Prandtl numbers are 0.025 and 0.71 where the working fluids are assumed to be mercury and air, respectively. It is shown that for both Prandtl numbers, very large-scale structures of the temperature fluctuations certainly exist in the outer layer at the given Reynolds numbers. Also, it is shown that at high Reynolds number, the very large-scale structures appear hierarchically in the outer layer for the two Prandtl numbers.

Introduction

The understanding of heat and mass, i.e. scalar, transport mechanism in wall turbulence is of great importance in both the scientific and the engineering viewpoints.

Experimental studies on turbulent heat transfer in wall-bounded flows have been performed over past several decades, and important aspects on the scalar transport mechanism have been reported in the literature. For example, Bremhorst and Bullock[1] measured cross-spectra of turbulent heat and momentum transfer in a turbulent pipe flow, and suggested an almost perfect correlation between the streamwise velocity and the temperature fluctuations at low wavenumbers. Fulachier and Dumas[2] conducted an experiment in a turbulent boundary layer. They showed that except in the buffer region the temperature spectrum differs strongly from the streamwise velocity spectrum, and the spectrum of three velocity components is similar to that of the temperature fluctuation. Perry and Hoffmann[3] made a measurement in a slightly heated boundary layer, and examined the scaling law on the mean and fluctuating temperature for the velocity and thermal fields. Subramanian and Antonia[4] conducted an experiment in a slightly heated boundary layer at $Re_\tau = u_\tau \delta / \nu = 371 \sim 2273$, where u_τ is the friction velocity, δ the channel half width or boundary layer thickness and ν the kinematic viscosity. They examined the Reynolds-number effect on mean temperature, temperature fluctuation, turbulent heat fluxes and turbulent Prandtl number. Antonia, Krishnamoorthy and Fulachier[5] investigated the correlation between the streamwise velocity and temperature fluctuations in the near-wall region. They indicated that the correlation coefficient of the streamwise turbulent heat-flux is large throughout the near-wall region, and its magnitude approaches unity at the wall.

On the other hand, owing to an evolution of numerical simulation technique, direct numerical simulation (DNS) has become an inevitable tool to examine turbulence phenomena. In wall turbulence, DNS of scalar transport has been first performed by Kim and Moin[6] in a turbulent channel flow at $Re_\tau = 180$ with $Pr = 0.2, 0.71$ and 2.0 using the uniform volumetric heating condition. Later, a lot of DNS studies on scalar transport have been performed in a turbulent channel flow at $Re_\tau = 150 \sim 180$ with

a wider range of Prandtl numbers, $Pr = 0.025 \sim 10.0$ [7-11], using various thermal boundary conditions, because the turbulent channel is simple in its geometry, and contains fundamental nature of wall turbulence. In these studies, the effects of the Prandtl number and of the thermal boundary conditions were fairly well examined. However, since these DNS studies were conducted at very low Reynolds numbers, the results obtained from DNS were not compared directly with the existing experimental results. Hence, there still remain several inconclusive issues such as Reynolds number dependence on turbulence statistics. Notably, the Reynolds-number effect on the peak values of the temperature variance and the turbulent heat-fluxes, and the behaviours of the turbulent Prandtl number and the time scale ratio have not reach a consensus because of the lack of sufficient information in the measurements.

Recently, with an aid of the development of computer power, DNS of a turbulent channel flow has been performed at relatively high Reynolds numbers. For the velocity field, the Reynolds-number effect on the root-mean-square velocity and vorticity fluctuations, and the scaling law of the energy spectra was carefully examined up to $Re_\tau = 1900$ (see, for example, Moser, Kim and Mansour[12], Abe, Kawamura and Matsuo[13], del Álamo, Jiménez, Zandonade and Moser[14]). Also, considering the experimental evidence that an importance of the outer-layer effect, i.e. large-scale structures, increases with increasing Reynolds number, the behaviour of large-scale structures was investigated by several researchers (see, for example, del Álamo and Jiménez[15], Abe, Kawamura and Choi[16]).

For the scalar field, on the other hand, DNS studies of Reynolds- and Prandtl-number effects on turbulence statistics were limited to $Re_\tau = 395$ (see, for example, Wikström and Johansson[17], Kawamura et al.[18, 19]), where firm conclusion on the Reynolds-number effect can hardly be drawn because the simulation at $Re_\tau = 180$ includes the low Reynolds-number effect (see, for example, Moser et al.[12]). Recently, the present author's group has established DNS database up to $Re_\tau = 1020$ with $Pr = 0.025$ and 0.71 using a constant heat-flux boundary condition, where the Reynolds number of $Re_\tau = 1020$ was chosen to be compared with the experimental results of Wei and Willmarth[20]. Using our DNS database, two DNS studies of turbulent heat transfer in a channel flow have been performed at $Re_\tau \geq 395$. Abe and Kawamura[21] reported turbulence thermal structures at $Re_\tau = 180 \sim 640$ with $Pr = 0.025$ and 0.71 . They showed that very large-scale structures of the temperature fluctuations appear clearly in the outer layer for $Re_\tau = 640$ at each Prandtl number. Abe, Kawamura and Matsuo[22] examined the Reynolds- and Prandtl-number effects on wall variables such as surface heat-flux fluctuations at $Re_\tau = 180 \sim 1020$ with $Pr = 0.025$ and 0.71 . They showed that the effect of large scales increases with increasing Reynolds number even in the wall variables. However, except these studies, the Reynolds- and Prandtl-number effects on turbulence statistics and turbulence structures for the scalar field have not been reported for $Re_\tau \geq 395$.

Re _τ	180	395	640	1020
Pr	0.025, 0.71	0.025, 0.71	0.025, 0.71	0.025, 0.71
L _x × L _y × L _z	12.8δ × 2δ × 6.4δ			
L _x × L _y × L _z	2304 × 360 × 1152	5056 × 790 × 2528	8192 × 1280 × 4096	13056 × 2040 × 6528
N _x × N _y × N _z	256 × 128 × 256	512 × 192 × 512	1024 × 256 × 1024	2048 × 448 × 1536
Δx ⁺ × Δy ⁺ × Δz ⁺	9.00, 0.20~5.90, 4.50	9.88, 0.15~6.52, 4.94	8.00, 0.15~8.02, 4.00	6.38, 0.15~7.32, 4.25
tu _m /L _x	49	50	14	10

Table 1. Computational box size, grid points, spatial resolution and sampling time period.

Therefore, in the present study, we use our DNS database of a fully developed turbulent channel flow with passive scalar transport up to Re_τ=1020 at Pr=0.025 and 0.71. The wide range of Reynolds numbers and two quite different Prandtl numbers allow us to evaluate the Reynolds- and Prandtl-number dependence adequately. The main objectives of the present study are to report the Reynolds- and Prandtl-number effects on very large-scale structures of the temperature fluctuations in the outer layer, which will appear clearly at high Reynolds number.

In this paper, numerical methodology is described in the following section. In the section of results and discussion, the first part is focused on the Reynolds- and Prandtl-number effects on the turbulence statistics, which exhibits fundamental statistical nature of wall turbulence at relatively high Reynolds numbers. On the other hand, the second part is on those of the very large-scale structures in the outer layer.

Numerical methodology

The governing equations for the velocity and scalar fields consist of the incompressible three-dimensional continuity, Navier-Stokes and energy equations. The flow is assumed to be a fully developed turbulent channel flow with a passive temperature field. It is driven by the streamwise mean pressure gradient. The temperature field is imposed through uniform heating on both walls, where the averaged heat flux is constant but the instantaneous one is time dependent.

The continuity and Navier-Stokes equations, respectively, are expressed as:

$$\frac{\partial u_i^+}{\partial x_i^*} = 0, \quad (1)$$

$$\frac{\partial u_i^+}{\partial t^*} + u_j^+ \frac{\partial u_i^+}{\partial x_j^*} = -\frac{\partial p^+}{\partial x_i^*} + \frac{1}{\text{Re}_\tau} \frac{\partial^2 u_i^+}{\partial x_j^{*2}} + \frac{\partial \bar{p}^+}{\partial x_i^*} \delta_{i1}, \quad (2)$$

which are non-dimensionalized by the friction velocity u_τ , the density ρ and the channel half width δ . Here, the variables u , p , t and x are the velocity, pressure, time and location, and the subscript $i=1, 2$ and 3 indicates the streamwise, wall-normal and spanwise directions, respectively. Note that the streamwise, wall-normal and spanwise velocities, u , v , and w , and the streamwise, wall-normal and spanwise locations, x , y , and z , are used interchangeably throughout this paper. The superscripts $+$ and $*$ indicate that the variables are normalized by wall units and the channel half width, respectively. The third term for right-hand side of Eq. (2) is the streamwise mean pressure gradient.

For the energy equation, the temperature difference θ is introduced to be satisfied with the constant heat-flux boundary condition. Since the statistically averaged temperature increases linearly in the streamwise direction, the instantaneous temperature $T^+(x^*, y^*, z^*)$ can be divided into the mean and fluctuating parts:

$$T(x^*, y^*, z^*) = \frac{d\langle \bar{T}_m^+ \rangle}{dx^*} x^* - \theta^+(x^*, y^*, z^*) \quad (3)$$

where $\langle \bar{T}_m^+ \rangle$ is the mixed mean temperature. Considering the present configuration, the first term for the right-hand side of Eq. (3) can be obtained as $d\langle \bar{T}_m^+ \rangle/dx^* = 2/\langle \bar{u}_1^+ \rangle$, where $\langle \bar{u}_1^+ \rangle$ is the

bulk mean velocity. Hence, using the above transformation, the energy equation is expressed as

$$\frac{\partial \theta^+}{\partial t^*} + u_j^+ \frac{\partial \theta^+}{\partial x_j^*} = \frac{1}{\text{Re}_\tau \cdot \text{Pr}} \frac{\partial^2 \theta^+}{\partial x_j^{*2}} + \frac{2u_1^+}{\langle \bar{u}_1^+ \rangle}. \quad (4)$$

Note that the temperature is normalized by the friction temperature $T_\tau (=Q_w/\rho c_p u_\tau)$, where Q_w and c_p denote the averaged surface heat-flux and the specific heat at constant pressure, respectively. In the x and z directions, the periodic boundary condition is employed. In the y direction, the non-slip and no temperature fluctuations conditions are used for the velocity and thermal fields, respectively, which are expressed as

$$u_i^+ = \theta^+ = 0 \quad (y = 0 \text{ and } 2\delta). \quad (5)$$

For the time integration, a fractional step method proposed by Dukowics and Dvinsky[23] is adopted, and a semi-implicit time advancement is used. For the viscous terms with wall-normal derivatives, the Crank-Nicolson method is used. For the other terms, the second-order Adams-Bashforth method is applied for Re_τ=180, 395 and 640, and the low storage third-order Runge-Kutta method (Spalart et al.[24]) for Re_τ=1020.

For the spatial discretization, the finite difference method is used. The numerical scheme proposed by Morinishi et al.[25] with the fourth-order accuracy is adopted in the streamwise and spanwise directions, whereas the second-order one is applied in the wall-normal direction. The computational box size (L_x, L_y, L_z), number of grid points (N_x, N_y, N_z), spatial resolution (Δ_x, Δ_y, Δ_z) and sampling time period (tu_m/L_x) are given in Table 1, where u_m denotes the bulk mean velocity. Detailed numerical methodology can be found in Kawamura et al.[18,19] and Abe et al.[13].

Results and discussion

Turbulence statistics

In the classical theory, the mean temperature $\bar{\theta}$ is expressed as

$$\frac{\bar{\theta}}{T_\tau} = f(y^+), \quad (6)$$

$$\frac{\bar{\theta}_c - \bar{\theta}}{T_\tau} = f\left(\frac{y}{\delta}\right), \quad (7)$$

where f and g represent the universal functions and the subscript c denotes the centreline value. The former and the latter are referred to as the law of the wall for the mean temperature and the temperature defect law, respectively. In our former work[22], we showed that the conductive sublayer follows the relation of Eq. (6), i.e. $\bar{\theta}^+ = \text{Pr} y^+$, for Re_τ=180~1020 at Pr=0.025 and 0.71. On the other hand, Hoffmann and Perry[26] suggested from their measurements that the temperature defect law, i.e. Eq. (7), is valid in the outer layer. Figure 1 shows the temperature defect law for the Reynolds and Prandtl numbers investigated. In Fig. 1, the temperature defect profile for Pr=0.71 indeed shows a good collapse in the outer layer, whereas that for Pr=0.025 shows a noticeable increase in the whole region with increasing Re_τ. The incomplete scaling for Pr=0.025 is due to the enhanced convective effect with increasing Reynolds number under the strong thermal conductive condition.

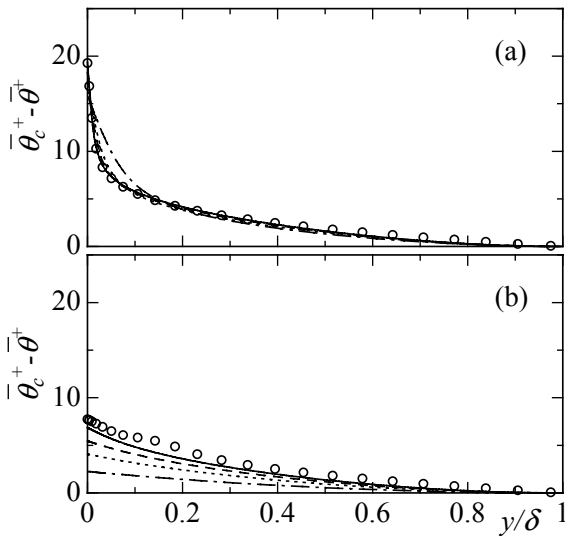


Figure 1. Temperature defect profile: (a) Pr=0.71; (b) Pr=0.025.
 —, Re_τ=1020; - - -, Re_τ=640; ·····, Re_τ=395;
 - · - ·, Re_τ=180; ○, Kader[27] for Re_τ=1020.

By integrating the area under the curve of the temperature defect profile, the Clauser thickness of the thermal boundary layer can be obtained as

$$\Delta_t = \int_0^1 \frac{\bar{\theta}_c - \bar{\theta}}{T_\tau} dy^* \quad (8)$$

The obtained Δ_t are summarized in Table 2, where the momentum Clauser thickness Δ is also included for comparison. It is shown in Table 2 that Δ_t for Pr=0.71 does not vary noticeably for the given Reynolds numbers, whereas that for Pr=0.025 increases appreciably with increasing Reynolds number. Also, it turns out from Table 2 that Δ_t for Pr=0.71 shows almost the same trend as Δ , indicating a high similarity between the velocity and thermal fields for each Reynolds number. On the other hand, Δ_t for Pr=0.025 differs noticeably from Δ independently of Re_τ, suggesting the breakdown of the similarity between the velocity and scalar fields, i.e. the Reynolds analogy.

The behaviour of the temperature fluctuations θ' is investigated using the probability density functions (PDFs). Figure 2 shows the PDFs of θ' for the Reynolds and Prandtl numbers examined at several wall-normal locations compared with those of the streamwise velocity fluctuations u' . In the case of Pr=0.71, near the wall, the peak position of the PDF deviates to the negative value, and the tail extends to the large magnitude of the positive value, indicating that the sweep occurs less frequently but it contributes more significantly to the heat transport. Moving away from the wall, the peak position of the PDF shifts gradually to the positive value, and the negative tail becomes more prominent with increasing y^+ . The Reynolds-number effect is noticeable in the positive and negative tails. As for the similarity between u' and θ' , the high similarity is observed near the wall, whereas the similarity decreases gradually moving away from the wall.

In the case of Pr=0.025, the PDFs below $y^+ \approx 10$ show almost the same behaviour independently of y^+ for each Re_τ due to the

Re _τ	Δ	Δ _θ	
		Pr=0.71	Pr=0.025
180	2.72	2.45	0.74
180[6]	2.7	2.4	-
395	2.69	2.34	1.27
640	2.72	2.43	1.64
1020	2.77	2.43	1.98

Table 2. Clauser thickness for the velocity and scalar fields.

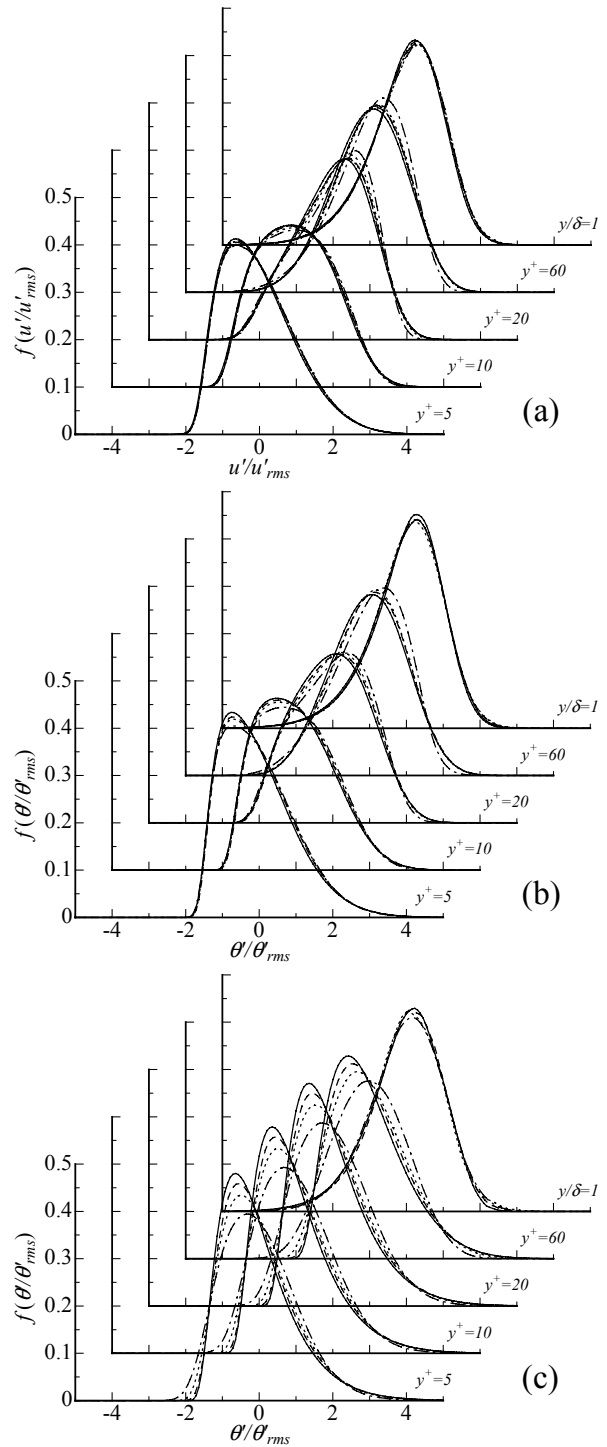


Figure 2. Probability density functions of u' and θ' :
 —, Re_τ=1020; - - -, Re_τ=640; ·····, Re_τ=395;
 - · - ·, Re_τ=180. (a) u' ; ·····, Moser et al.[12] for Re_τ=590;
 (b) θ' for Pr=0.71; (c) θ' for Pr=0.025.

strong conductive effect. Also, near the wall, the significant Reynolds-number effect appears. That is, the PDF is more positively skewed with increasing Re_τ due to the enhanced convective effect. In the central region, on the other hand, the PDF is negatively skewed, and the Reynolds-number dependence is rather small.

The streamwise turbulent heat flux $\overline{u''\theta''}$ and its cross-correlation coefficient $R_{u\theta} (= \overline{u''\theta''} / u'_{rms} \theta'_{rms})$ are given in Figs. 3 and 4, respectively, where the subscript *rms* denotes the root-mean-square value. It is shown in Fig. 3 that the peak value of $\overline{u''\theta''}$ increases with increasing Reynolds number for each Pr.

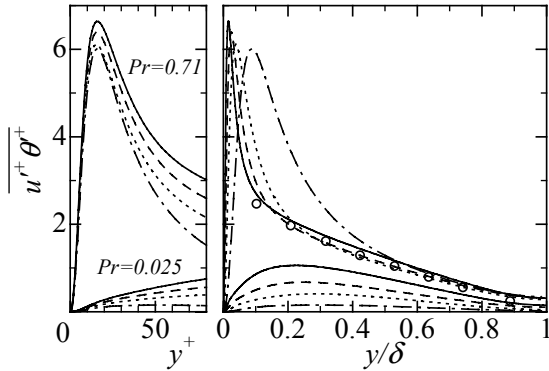


Figure 3. Streamwise turbulent heat flux: —, $Re_\tau=1020$; - - -, $Re_\tau=640$; , $Re_\tau=395$; - · - · , $Re_\tau=180$; ○ , Subramanian and Antonia[4] for $Re_\tau \approx 1055$.

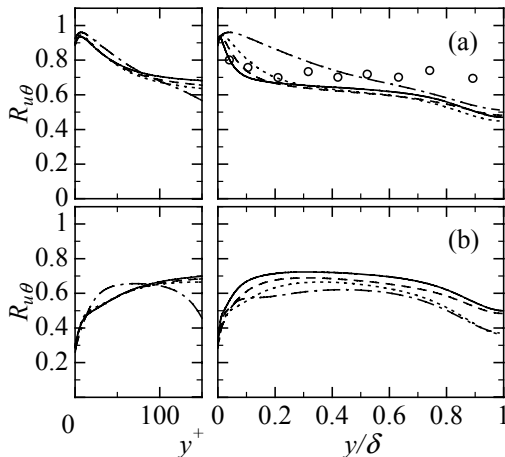


Figure 4. Correlation coefficient of the streamwise turbulent heat flux: (a) $Pr=0.71$; (b) $Pr=0.025$. —, $Re_\tau=1020$; - - -, $Re_\tau=640$; , $Re_\tau=395$; - · - · , $Re_\tau=180$; ○ , Subramanian and Antonia[4] for $Re_\tau \approx 1055$.

The increasing rate for $Pr=0.025$ from $Re_\tau=180$ to 1020 is larger than that for $Pr=0.71$, indicating that the enhancement of the convective effect due to the increase in Re_τ is more significant in the low Pr fluid than in the medium to high Pr one. Also, considering no constrained condition in the streamwise direction, the peak value of $u'+\theta'+$ may continue to increase with increasing Reynolds number for both Pr cases.

In Fig. 4, the cross-correlation coefficient $R_{u\theta}$ exhibits a quite different behaviour in the near wall region for each Pr . That is, $R_{u\theta}$ for $Pr=0.71$ shows a clear peak near the wall and decreases gradually toward the outer layer, whereas that for $Pr=0.025$ shows no clear peak near the wall and increases gradually toward the outer layer. This difference must be attributed to the fact that θ' for $Pr=0.71$ is a near-wall marker, whereas that for $Pr=0.025$ marks in a wider range of the flow region. However, in spite of these different characteristics of θ' , $R_{u\theta}$ is scaled well with the inner variables at $y^+ \leq 50$ for each Pr over $Re_\tau=395$. Also, we see that for $Pr=0.71$, the clear peak appears at $y^+ \approx 7$ regardless of Re_τ , and its peak value remains unchanged as 0.94 over $Re_\tau=395$, suggesting that near the wall, the high similarity between u' and θ' at $Pr=0.71$ does not change substantially over $Re_\tau=395$.

The wall-normal turbulent heat flux $-v''\theta''$ and its cross-correlation coefficient $-R_{v\theta} (= -\overline{v'\theta'}/v'_{rms}\theta'_{rms})$ are shown in Figs. 5 and 6, respectively. In Fig. 5, the total heat flux Q_{total} and the temperature gradient, i.e. molecular heat flux, $(1/Pr)(d\bar{\theta}/dy^+)$, are also included. It can be confirmed in Fig. 5 that for all the cases investigated, the total heat-flux reaches the

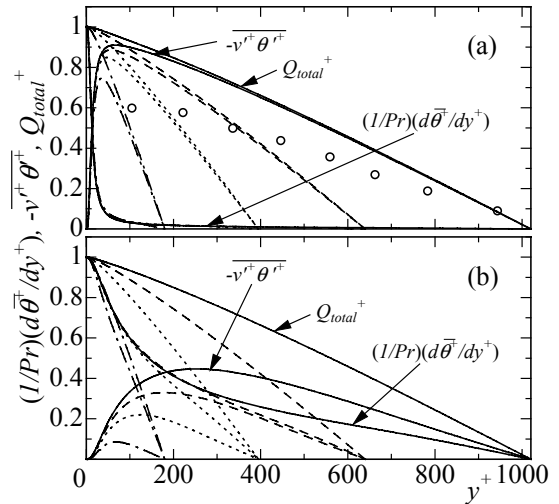


Figure 5. Wall-normal turbulent heat flux: —, $Re_\tau=1020$; - - -, $Re_\tau=640$; , $Re_\tau=395$; - · - · , $Re_\tau=180$; ○ , Subramanian and Antonia[4] for $Re_\tau \approx 1055$.

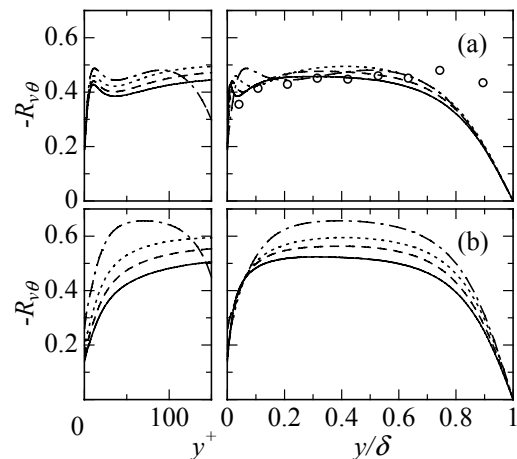


Figure 6. Correlation coefficient of the wall-normal turbulent heat flux: (a) $Pr=0.71$; (b) $Pr=0.025$. —, $Re_\tau=1020$; - - -, $Re_\tau=640$; , $Re_\tau=395$; - · - · , $Re_\tau=180$; ○ , Subramanian and Antonia[4] for $Re_\tau \approx 1055$.

statistically steady state, indicating that the sampling average time is quite sufficient to discuss the Reynolds- and Prandtl-number effects on the turbulence statistics.

In Fig. 5, with increasing Re_τ , the peak value of $-v''\theta''$ increases and its peak position moves toward a larger y^+ for each Prandtl number. In the case of $Re_\tau=1020$, the peak value of $-v''\theta''$ is 0.90 ($y^+ = 67$) and 0.45 ($y^+ = 254$) for $Pr = 0.71$ and 0.025 , respectively. Interestingly, for $Pr=0.025$, the turbulent heat flux exceeds the molecular heat flux at $y^+ > 200$ when Re_τ reaches 1020 , although the molecular contribution is still large throughout the channel at the given Reynolds numbers.

As for the cross-correlation coefficient $-R_{v\theta}$, a large difference between $Pr=0.025$ and 0.71 exist in the near-wall region as seen in the behaviour of $R_{u\theta}$. For $Pr=0.71$, a close similarity between $-R_{v\theta}$ and $-R_{uv}$ (not shown here) is found near the wall independently of Re_τ , suggesting that $-v''\theta''$ and $-u''v''$ are generated by approximately the same turbulence transport mechanism there. Also, the agreement between the present result and that of Subramanian and Antonia[4] is good except for the centre of the channel where flow characteristics between the channel and boundary layers are quite different. For $Pr=0.025$, on the other hand, $-R_{v\theta}$ shows a lower value than that for $Pr=0.71$

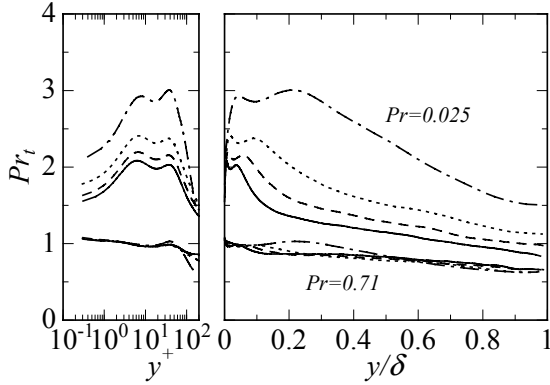


Figure 7. Turbulent Prandtl number; —, $Re_\tau=1020$; - - -, $Re_\tau=640$; , $Re_\tau=395$; - · - · , $Re_\tau=180$.

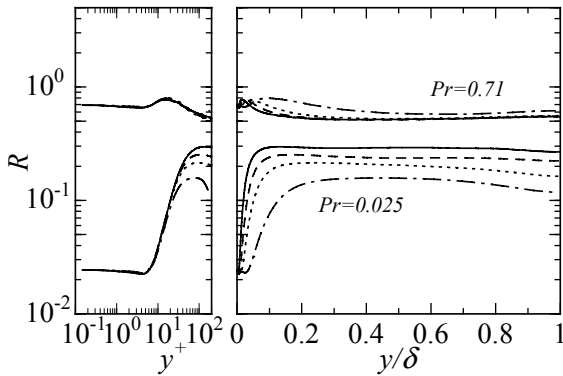


Figure 8. Time scale ratio; —, $Re_\tau=1020$; - - -, $Re_\tau=640$; , $Re_\tau=395$; - · - · , $Re_\tau=180$.

near the wall and increases gradually toward the outer layer. Interestingly, in the outer layer, $-R_{v\theta}$ decreases gradually with increasing Re_τ due to the enhanced convective effect, which is in contrast to the behaviour of $R_{u\theta}$ (see Figs. 4(b) and 6(b)).

Turbulent Prandtl number is defined as

$$Pr_t = \frac{\nu_t}{\alpha_t} = \frac{\overline{u^+ v^+}}{\overline{v^+ \theta^+}} \cdot \frac{(d\overline{\theta^+} / dy^+)}{(d\overline{u^+} / dy^+)}, \quad (9)$$

which corresponds to the ratio of turbulent eddy viscosity ν_t to thermal eddy diffusivity α_t . Figure 7 shows the turbulent Prandtl number for the Reynolds and Prandtl numbers calculated. For $Pr = 0.71$, as the wall is approached, Pr_t tends to be a constant value of 1.1 independently of Re_τ . This coincides well with the low Re DNS results of Kim and Moin[6] and Antonia and Kim[28] in the channel flow with the uniform volumetric heating and that of Kong, Choi, and Lee[29] in the thermal boundary layer. In the centre of the channel, Pr_t decreases down to 0.65 independently of Reynolds number. Interestingly, in the case of $Re_\tau=1020$, Pr_t stays at a roughly constant value of 0.86 at $0.1 < y/\delta < 0.4$. This is very close to the value of 0.9 which was often used in the calculation of turbulent heat transfer using turbulence modelling.

For $Pr = 0.025$, on the other hand, Pr_t shows a larger value than that of $Pr = 0.71$ for all the Reynolds numbers. Nevertheless, with increasing Re_τ , Pr_t decreases appreciably and tends to approach unity. One may wonder if the near-wall limiting value of Pr_t for $Pr=0.025$ also asymptotes to unity for extremely high Re . Considering the quite different behaviour of $-R_{v\theta}$ between $Pr=0.025$ and 0.71 in the near-wall region (see Fig. 6), it may be concluded that the near-wall value of Pr_t for $Pr=0.025$ does not asymptote to unity for high Reynolds number.

With respect to the scaling law for Pr_t , in the case of $Pr=0.71$, the inner scaling is valid up to $y^+=100$, while the outer one is in

the range, $0.2 < y/\delta < 1$, except for $Re_\tau=180$. On the other hand, in the case of $Pr=0.025$, no collapse is observed for the Reynolds number range investigated.

The time scale ratio is a quantity often used to estimate the dissipation rate of the temperature variance. It is defined as

$$R = \frac{\tau_\theta}{\tau_u} = \frac{\overline{\theta'^{r+2}} \varepsilon}{2k\varepsilon_\theta}. \quad (10)$$

Its wall asymptotic value is analytically equal to the molecular Prandtl number. Figure 8 shows the distribution of the time scale ratio for the given Reynolds and Prandtl numbers. Near-the wall, the limiting value of R becomes indeed Pr irrespective of Reynolds number. In the outer layer, the time scale ratio for $Pr=0.71$ shows a good collapse with the outer scaling in the range, $0.2 < y/\delta < 1$, where R stays 0.5~0.6 and shows an almost plateau. This value is very close to that of 0.5, which was often used in earlier turbulence modelling to obtain the dissipation rate of the temperature variance[30]. On the other hand, time scale ratio for $Pr=0.025$ does not collapse for the given Reynolds numbers. Nevertheless, it is interesting to note that R tends to approach 0.5 with increasing Reynolds number even at $Pr=0.025$.

Very large-scale structures

The large-scale structures are often referred to as the large-scale motions existing in the outer layer of the flow, and many experimental studies on the large-scale motions have been conducted for turbulent pipe, boundary layer and channel flows (see, for example, Kim and Adrian[31]; Adrian et al.[32]; Liu et al.[33]). Furthermore, Kim and Adrian[31] found that very large-scale motions which are much longer than the large-scale motions exist in the outer layer in a turbulent pipe flow.

Recently, DNS of turbulent channel flow at relatively high Reynolds numbers showed convincing evidence on very large-scale structures in the outer layer. For the velocity field, del Álamo and Jiménez[15] found that very large-scale structures of u' appear at $y/\delta=0.5$ for $Re_\tau=180$ and 550, where the streamwise and spanwise size is about 5δ and 2δ , respectively. Abe, Kawamura and Choi[16] obtained the most energetic spanwise scale as 1.3~1.6 δ for $Re_\tau=180$ ~640. For the thermal field, Abe and Kawamura[21] reported from their DNS results that there exist very large-scale structures of θ' in the outer layer for $Re_\tau=640$ with $Pr=0.025$ and 0.71. However, the spanwise organization of the very large-scale structures of θ' has not been examined in detail. Therefore, we investigate here the behaviour of the very large-scale structures in the spanwise direction.

One-dimensional spanwise wavenumber energy spectra of the temperature fluctuations θ' are defined as

$$\int_0^\infty \phi(k_z) dk_z = \theta'_{rms}{}^2, \quad (11)$$

where k_z is the spanwise wavenumber and λ_z the corresponding wavelength. The spanwise pre-multiplied energy spectra of the temperature fluctuations for $Re_\tau=180, 395, 640$ and 1020 at $Pr=0.025$ and 0.71 are given in Figs. 9 and 10, where spectral peaks at long wavelengths appear more clearly for high Reynolds number. Note that the wavelength where the pre-multiplied energy spectrum shows a maximum indicates the most energetic scale. In the case of $Pr=0.71$, with increasing Re_τ , spanwise length scales are separated clearly, and small and large scales are scaled with the inner and outer variables, respectively. Near the wall, a clear peak appears at $\lambda_z^+ \approx 100$ for each Reynolds number. Away from the wall, the peak moves to longer wavelengths. At $y/\delta=0.5$, a large peak appears at $\lambda_z/\delta=1.3$ ~1.6 for all the Re_τ , suggesting an existence of very large-scale structures of θ' in the outer layer. This trend is also observed in the spanwise spectra of u' (not shown here). However, comparison of the spectra between u' and θ' shows that the peak value of θ' is much

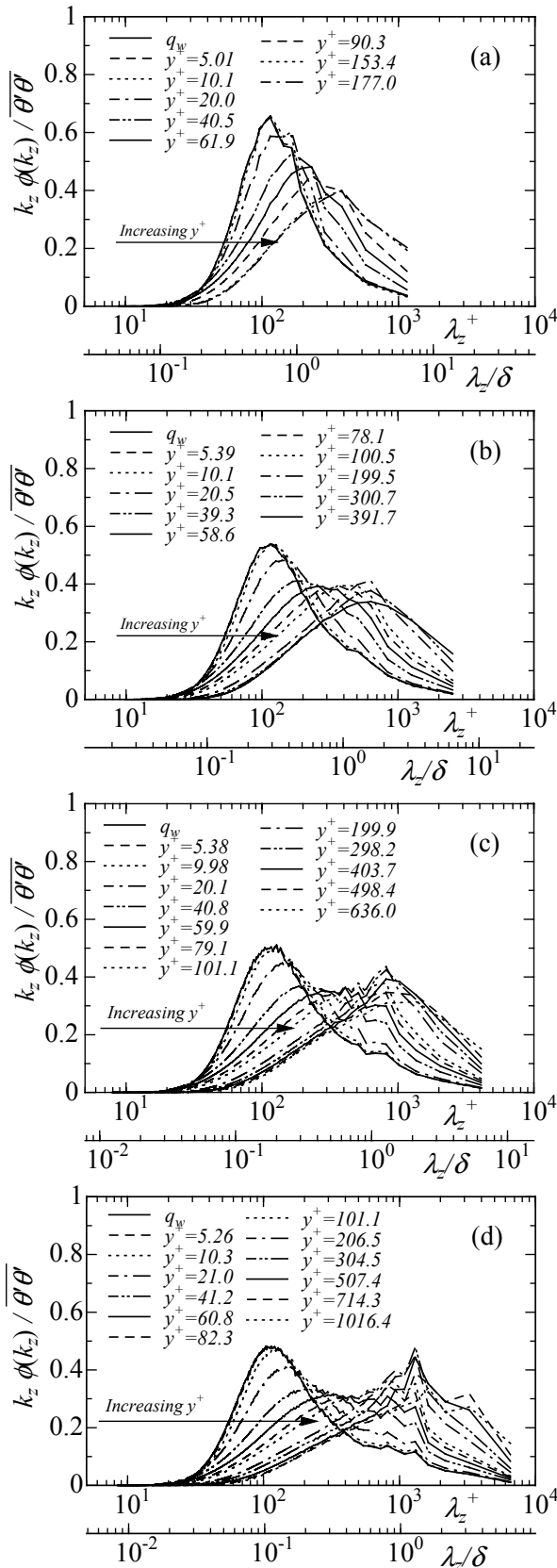


Figure 9. Spanwise pre-multiplied energy spectra of θ' at $Pr=0.71$: (a) $Re_\tau=180$; (b) $Re_\tau=395$; (c) $Re_\tau=640$; $Re_\tau=1020$.

smaller than that of u' in the outer layer, indicating a dissimilarity in the very large-scale structures between u' and θ' . In the case of $Pr=0.025$, on the other hand, all the spectral peaks appear at long wavelengths regardless of y^+ for all the Reynolds numbers. This may be yielded by the strong conductive effect throughout the channel. Interestingly, in the case of $Re_\tau=1020$, another large

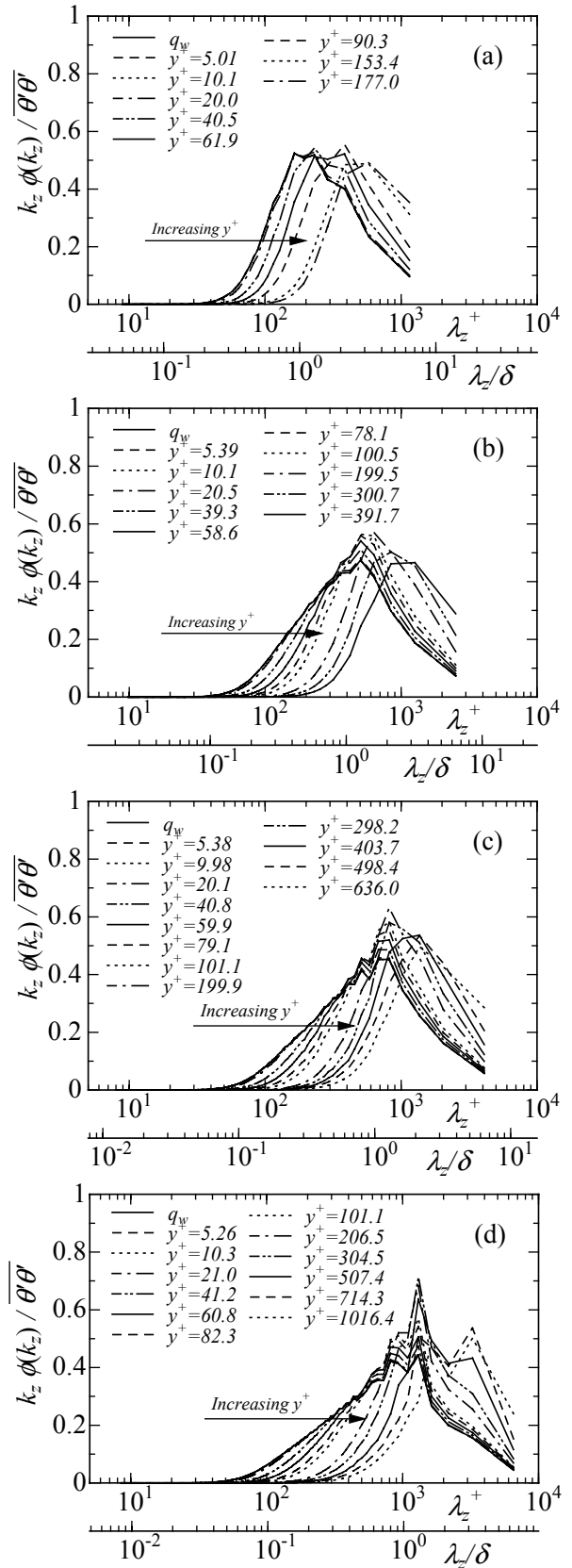


Figure 10. Spanwise pre-multiplied energy spectra of θ' at $Pr=0.025$: (a) $Re_\tau=180$; (b) $Re_\tau=395$; (c) $Re_\tau=640$; $Re_\tau=1020$.

peak appears at a long wavelength, $\lambda_z/\delta \approx 0.9$, at $y^+ \approx 0.2$ for the both Pr cases. Since this peak does not appear clearly at $Re_\tau \leq 640$, it may be closely associated with the enhanced nonlinear effect with increasing Re_τ , indicating that there exist hierarchical very large-scale structures of θ' in the outer layer at high Reynolds number for the two Pr fluids.

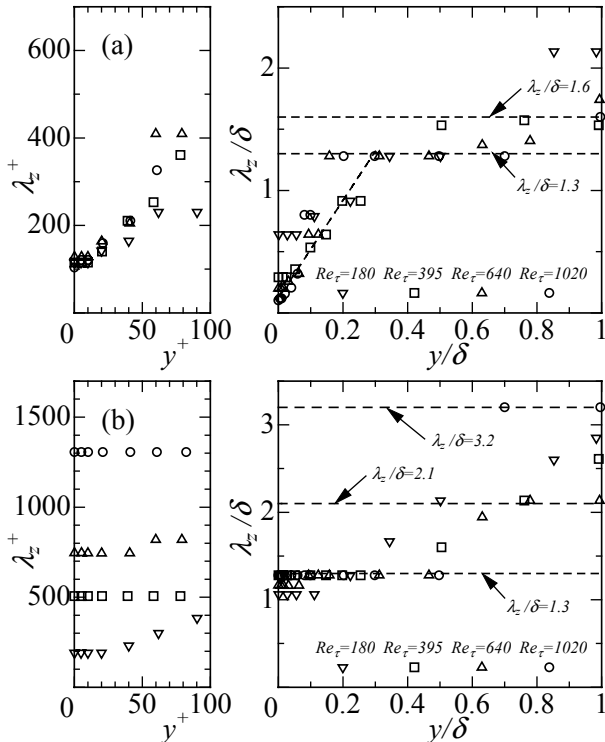


Figure 11. The most energetic spanwise wavelengths obtained from the pre-multiplied energy spectra of θ' for $Re_\tau=180, 395, 640$ and 1020 : (a) $Pr=0.71$; (b) $Pr=0.025$.

The most energetic wavelengths (MEWs, hereafter) of θ' are obtained from Figs. 9 and 10, and are presented in Fig. 11. Note that when the pre-multiplied spanwise spectrum shows a clear peak we have taken the most energetic wavelength, while when the spectrum shows a broad peak we have computed a least-square interpolating polynomial in the region where the spectrum shows the most energetic power. In Fig. 11, there appears a significant Pr dependence independently of Reynolds number. For $Pr=0.71$, the MEWs can be divided into three regions. Near the wall ($y^+ < 10$), we see the MEWs at $\lambda_z^+ \approx 100$. Away from the wall ($y^+ > 10, y/\delta < 0.3$), the MEWs increase linearly with distance from the wall. In the outer layer ($0.3 < y/\delta < 1$), the MEWs stay $1.3 \sim 1.6\delta$ and show an almost plateau. On the other hand, for $Pr=0.025$, the MEWs can be categorized into two regions. Below $y/\delta=0.5$, the MEWs are obtained as $1.3 \sim 2.1\delta$, while those are $2.1 \sim 3.2\delta$, indicating that in the very low Pr fluid, only large-scale structures exist even in the near-wall region independently of Re_τ .

We will show the variation of the very large-scale structures of θ' as a function of the Reynolds number. The instantaneous temperature fluctuations for $Re_\tau=180$ and 1020 at $Pr=0.71$ are normalized by their own rms values at each y^+ , and are shown in Fig. 12. This normalization allows us to evaluate the outer-layer structures adequately [16, 22]. Note that for Fig. 12(c), only the data in the range, $y/\delta=0 \sim 0.2$, are visualized in order to show instantaneous evidence of hierarchical very large-scale structures in the outer layer at high Reynolds number. It is obvious from Figs. 12(a) and (b) that for each Re_τ , large-scale positive and negative temperature fluctuations appear alternatively in the spanwise direction. The spanwise spacing of the negative θ' is about $1.3 \sim 1.6\delta$ at $y/\delta \approx 0.5$, which agrees well with the wavelengths at which the spanwise pre-multiplied spectra show maxima in the outer layer. With increasing Re_τ , very large-scale structures with wider scales appear in the outer layer, as expected. For $Re_\tau=1020$, another large-scale structures with a spanwise spacing, $0.8 \sim 1.0\delta$ appear at $y/\delta \approx 0.2$ (see Fig. 12(c)), suggesting the existence of the hierarchical very large-scale structures. Furthermore, the very large-scale structures of θ' show much

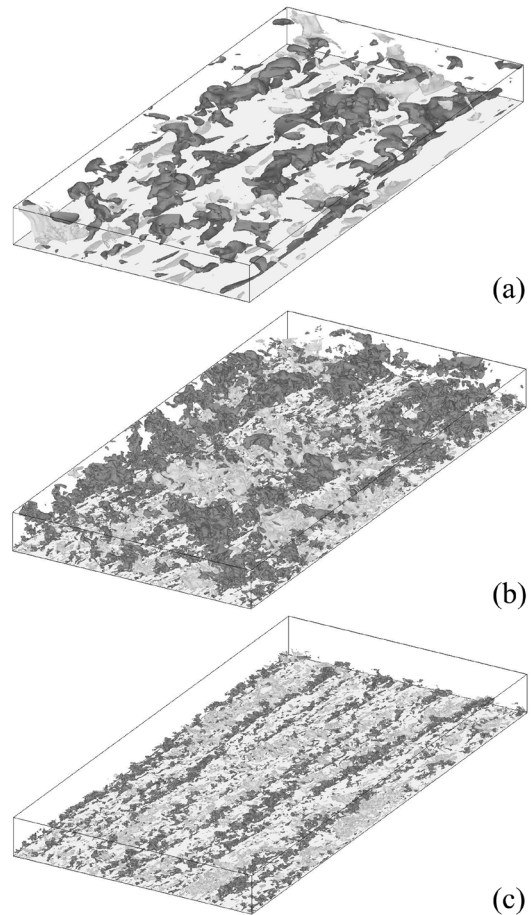


Figure 12. Iso-surfaces of the instantaneous temperature fluctuations normalized by their own rms value at each y^+ for $Re_\tau=180$ and 1020 at $Pr=0.71$: (a) $Re_\tau=180$; (b) $Re_\tau=1020$; (c) $Re_\tau=1020$ (plotted in the range, $y/\delta=0 \sim 0.2$). Light-gray, $\theta'/\theta'_{rms} > 1.75$; dark-gray, $\theta'/\theta'_{rms} < -1.75$. The boxes visualized here are $12.8\delta \times \delta \times 6.4\delta$ in x, y and z directions. The direction of the flow is from bottom-left to top-right.

sharper gradient to the wall as compared with those of u' (not shown here). This temperature structure may be closely related to the temperature front reported by Chen and Blackwelder [34].

Similarly, the instantaneous temperature fluctuations for $Re_\tau=180$ and 1020 at $Pr=0.025$ are normalized by their own rms values at each y^+ , and are shown in Fig. 13. Indeed, very large-scale structures with a spanwise spacing, $1.3 \sim 1.6\delta$, exist in the outer layer for each Re_τ . Interestingly, the shapes of the structures do not change noticeably with increasing Re_τ . Also, in the case of $Re_\tau=1020$, hierarchical very large-scale structures appear in the outer layer, as was shown at $Pr=0.71$.

Conclusions

In the present study, we performed DNS of turbulent channel flow with passive scalar transport at $Re_\tau=180, 395, 640$ and 1020 with $Pr=0.025$ and 0.71 , and investigated the Reynolds- and Prandtl-number effects on the turbulence statistics and the very large-scale structures existing in the outer layer of the flow.

An investigation of the turbulence statistics showed that near the wall, the turbulent Prandtl number for $Pr=0.71$ becomes 1.1 independently of Re_τ , whereas that for $Pr=0.025$ does not asymptote to unity even for $Re_\tau=1020$. Also, the near-wall limiting value of the time scale ratio becomes indeed Pr irrespective of Reynolds number. In the outer layer, Pr_t and R for $Pr=0.71$ scale with the outer variable in the range, $0.2 < y/\delta < 1$.

An inspection of the very large-scale structures of θ' in the outer layer revealed that for all the Reynolds numbers, there certainly exist very large-scale structures with a spanwise spacing,

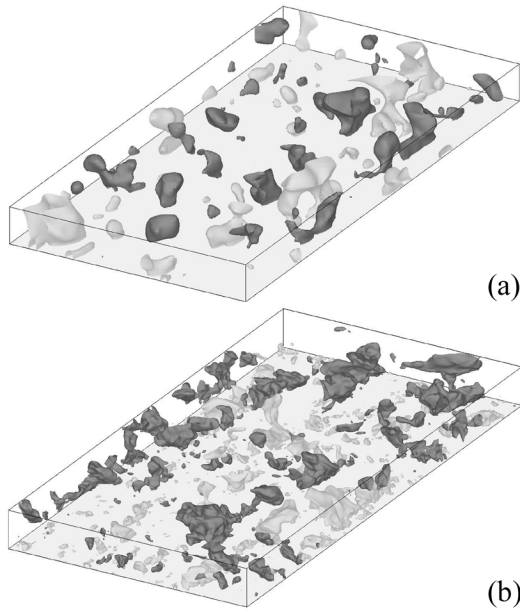


Figure 13. Iso-surfaces of the instantaneous temperature fluctuations normalized by their own rms value at each y^+ for $Re_\tau=180$ and 1020 at $Pr=0.025$: (a) $Re_\tau=180$; (b) $Re_\tau=1020$. Light-gray, $\theta'/\theta'_{rms} > 1.75$; dark-gray, $\theta'/\theta'_{rms} < -1.75$. The boxes visualized here are $12.8\delta \times \delta \times 6.4\delta$ in x , y and z directions. The direction of the flow is from bottom-left to top-right.

$1.3 \sim 1.6\delta$ at $y/\delta \approx 0.5$ at the two Pr cases. Also, in the case of $Re_\tau=1020$, another large-scale structures with a spanwise spacing, $0.8 \sim 1.0\delta$, appear at $y/\delta \approx 0.2$. This indicates that hierarchical very large-scale structures exist in the outer layer, which may be closely associated with the enhanced nonlinear effect with increasing Reynolds number.

Ensemble averaged statistics are/will be presented at <http://murasun.me.noda.tus.ac.jp>.

Acknowledgments

Computations were made with Numerical Simulator III at Computer Center of Japan Aerospace Exploration Agency, and also VPP5000 at Tokyo University of Science and Computer Center of Kyushu University.

References

[1] Bremhorst, K. and Bullock, K., Spectral measurements of turbulent heat and momentum transfer in fully developed pipe flow, *Int. J. Heat Mass Transfer*, **16**, 1973, 2141-2154.
 [2] Fulachier, L. and Dumas, R., Spectral analogy between temperature and velocity fluctuations in a turbulent boundary layer, *J. Fluid Mech.*, **77**, 1976, 257-277.
 [3] Perry, A. E. and Hoffmann, P. H., An experimental study of turbulent convective heat transfer from a flat plate, *J. Fluid Mech.*, **77**, 1976, 355-368.
 [4] Subramanian, C. S. and Antonia, R. A., Effect of Reynolds number on a slightly heated turbulent boundary layer, *Int. J. Heat Mass Transfer*, **24**, 1981, 1833-1846.
 [5] Antonia, R. A., Krishnamoorthy, L. V. and Fulachier, L., Correlation between the longitudinal velocity fluctuation and temperature fluctuation in the near-wall region of a turbulent boundary layer, *Int. J. Heat Mass Transfer*, **31**, 1988, 723-730.
 [6] Kim, J. and Moin, P., Transport of passive scalars in a turbulent channel flow, in *Turbulent shear flows 6*, editors J.-C. André et al., Springer-Verlag, Berlin, 1989, 85-96.
 [7] Lyons, S. L., Hanratty, T. J., and McLaughlin, J. B., Direct numerical simulation of passive heat transfer in a turbulent channel flow, *Int. J. Heat Mass Transfer*, **34**, 1991, 1149-1161.
 [8] Kasagi, N., Tomita, Y., and Kuroda, A., Direct numerical simulation of passive scalar field in a turbulent channel flow, *ASME J. Heat Transfer*, **114**, 1992, 598-606.
 [9] Kasagi, N. and Ohtsubo, Y., Direct numerical simulation of low Prandtl number thermal field in a turbulent channel flow, in

Turbulent shear flows 8, editors F. Durst et al., Springer-Verlag, Berlin, 1993, 97-119.
 [10] Kawamura, H., Ohsaka, K., Abe, H., and Yamamoto, K., DNS of turbulent heat transfer in channel flow with low to medium-high Prandtl number fluid, *Int. J. Heat and Fluid Flow*, **19**, 1998, 482-491.
 [11] Na, Y. and Hanratty, T. J., Limiting behavior of turbulent scalar transport close to a wall, *Int. J. Heat Mass Transfer*, **43**, 2000, 1749-1758.
 [12] Moser, R. D., Kim, J., and Mansour, N. N., Direct numerical simulation of turbulent channel flow up to $Re_\tau=590$, *Phys. Fluids*, **11**, 1999, 943-945.
 [13] Abe, H., Kawamura, H., and Matsuo, Y., Direct numerical simulation of a fully developed turbulent channel flow with respect to the Reynolds number dependence, *ASME J. Fluids Eng.*, **123**, 2001, 382-393.
 [14] del Álamo, J. C. and Jiménez, J., Spectra of the very large anisotropic scales in turbulent channels, *Phys. Fluids*, **15**, 2003, L41-L44.
 [15] del Álamo, J. C., Jiménez, J., Zandonade, P., and Moser, R. D., Scaling of the energy spectra of turbulent channels, *J. Fluid Mech.*, **500**, 2004, 135-144.
 [16] Abe, H., Kawamura, H., and Choi, H., Very large-scale structures and their effects on the wall shear-stress fluctuations in a turbulent channel flow up to $Re_\tau=640$, *ASME J. Fluids Eng.*, 2004, to appear.
 [17] Wikström, P. M. and Johansson, A. V., DNS and scalar-flux transport modeling in a turbulent channel flow, in *Proc. of 2nd EF Conference in Turbulent Heat Transfer*, vol. 1, Manchester, UK, 1998, 6.46-6.51.
 [18] Kawamura, H., Abe, H. and Matsuo, Y., DNS of turbulent heat transfer in channel flow with respect to Reynolds and Prandtl number effects, *Int. J. Heat and Fluid Flow*, **20**, 1999, 196-207.
 [19] Kawamura, H., Abe, H., and Shingai, K., DNS of turbulence and heat transport in a channel flow with different Reynolds and Prandtl numbers and boundary conditions, in *Proc. of 3rd Int. Symp. Turbulence, Heat and Mass Transfer*, editors Y. Nagano et al., 2000, 15-32.
 [20] Wei, T. and Willmarth, W. W., Reynolds-number effects on the structures of a turbulent channel flow, *J. Fluid Mech.*, **204**, 1989, 57-95.
 [21] Abe, H. and Kawamura, H., A study of turbulence thermal structure in a channel flow through DNS up to $Re_\tau=640$ with $Pr=0.025$ and 0.71 , in *Proc. of 9th European Turbulence Conference*, 2002, 399-402.
 [22] Abe, H., Kawamura, H., and Matsuo, Y., Surface heat-flux fluctuations in a turbulent channel flow up to $Re_\tau=1020$ with $Pr=0.025$ and 0.71 , *Int. J. Heat and Fluid Flow*, **25**, 2004, 404-419.
 [23] Dukowicz, J. K. and Dvinsky, A. S., Approximate factorization as a high order splitting for the implicit incompressible flow equations, *J. Comp. Phys.*, **102**, 1992, 336-347.
 [24] Spalart, P. R., Moser, R. D., and Rogers, M. M., Spectral methods for the Navier-Stokes equations with one infinite and two periodic directions, *J. Comp. Phys.*, **96**, 1991, 297-324.
 [25] Morinishi, Y., Lund, T. S., Vasilyev, O. V., and Moin, P., Fully conservative higher order finite difference schemes for incompressible flow, *J. Comp. Phys.*, **143**, 1998, 90-124.
 [26] Hoffmann, P. H. and Perry, A. E., The development of thermal boundary layers on flat plates, *Int. J. Heat Mass Transfer*, **22**, 1979, 39-46.
 [27] Kader, B. A., Temperature and concentration profiles in fully turbulent boundary layers, *Int. J. Heat Mass Transfer*, **24**, 1981, 1541-1544.
 [28] Antonia, R. A. and Kim, J., Turbulent Prandtl number in the near-wall region of a turbulent channel flow, *Int. J. Heat Mass Transfer*, **34**, 1991, 1905-1908.
 [29] Kong, H., Choi, H., and Lee, J. S., Direct numerical simulation of turbulent thermal boundary layers, *Phys. Fluids*, **12**, 2000, 2555-2568.
 [30] Béguier, C., Dekeyser, I., and Launder, B. E., Ratio of scalar and velocity dissipation time scales in shear flow turbulence, *Phys. Fluids*, **21**, 1978, 307-310.
 [31] Kim, K. C. and Adrian, R. J., Very large-scale motion in the outer layer, *Phys. Fluids*, **11**, 1999, 417-422.
 [32] Adrian, R. J., Meinhart, C. D. and Tomkins, C. D., Vortex organization in the outer layer region of the turbulent boundary layer, *J. Fluid Mech.*, **422**, 2000, 1-54.
 [33] Liu, Z., Adrian, R. J. and Hanratty, T. J., Large-scale modes of turbulent channel flow: transport and structure, *J. Fluid Mech.*, **448**, 2001, 53-80.
 [34] Chen, C.-H.P. and Blackwelder, R. F., Large-scale motion in a turbulent boundary layer: a study using temperature contamination, *J. Fluid Mech.*, **89**, 1978, 1-31.